Bioactive Materials 20 (2023) 651–662

Contents lists available at ScienceDirect

Bioactive Materials

journal homepage: www.keaipublishing.com/en/journals/bioactive-materials

A breakthrough trial of an artificial liver without systemic heparinization in hyperbilirubinemia beagle models

Yilin Wang [a,b], Shanshan Wang [a,b], Xueqin He [c], Yupei Li [c], Tao Xu [a,b], Lin Xu [a,b], Bo Yang [a,b], Xinnian Fan [a], Weifeng Zhao [a,b,*], Changsheng Zhao [a,b,**]

[a] College of Polymer Science and Engineering, State Key Laboratory of Polymer Materials Engineering, Sichuan University, Chengdu, 610065, China
[b] Med-X Center for Materials, Sichuan University, Chengdu, 610041, China
[c] Department of Nephrology, West China Hospital, Sichuan University, Chengdu, 610041, China

ARTICLE INFO

Keywords:
Wearable artificial liver
Anticoagulant
Bilirubin
Kevlar
Microspheres

ABSTRACT

The development of wearable artificial livers was restricted to device miniaturization and bleeding risk with water-soluble anticoagulants. Herein, a double-deck column filled with solid anticoagulant microspheres and Kevlar porous microspheres (KPMs, bilirubin adsorbents) was connected with the principle machine of wearable artificial liver (approximately 9 kg) to treat hyperbilirubinemia beagles for the first time. With the initial normal dose of heparin, the double-deck column could afford 3 h hemoperfusion in whole blood without thrombus formation. The removal efficiency of the double-deck column for total bilirubin (TBIL) was 31.4%. Interestingly, the excessive amounts of hepatocyte metabolites were also decreased by approximately 25%. The "anticoagulant + column" realized safe and effective whole blood hemoperfusion without the plasma separation system and heparin pump; however, the proposed principle machine of wearable artificial liver and "anticoagulant + column" cannot completely replace the bio-liver now. The intelligence of the device and the versatility of the adsorbent need to be improved; moreover, advanced experimental techniques need to be developed to validate the survival rates in animals. Overall, this study is a meaningful trial for the development of wearable artificial livers in the future.

1. Introduction

Liver failure is a group of clinical syndromes characterized by coagulation mechanism disorder, jaundice, hepatic encephalopathy and respiratory failure [1]. Bilirubin is a crucial toxin in liver metabolism and an indicator of liver function [2]. It is a tetrapyrrolic compound originating from heme catabolism [3]. Adult patients with liver failure are unable to properly metabolize or excrete bilirubin, resulting in hyperbilirubinemia [4]. Commonly, the therapies for patients are basic medical treatment and artificial liver support therapy before they find suitable liver sources [5,6]. However, orthotopic liver transplantation is limited by rare organ donors, immunological rejection and expensive medical expenses. Therefore, the artificial liver support system is still the best choice [7,8].

Generally, patients need to go to the hospital at least two or three times a week for artificial liver support system therapy to survive, which greatly reduces the quality of life and places a huge economic burden on patients [9]. Therefore, Shirane et al. envisioned a wearable artificial liver in the 1970s [10]. Regretfully, such a wearable artificial liver device is not yet available. The development of wearable artificial livers is facing three major problems. (1) Anticoagulant medications are frequently used to prevent coagulation during blood purification. However, patients with liver failure often suffer from coagulation disorders, and water-soluble anticoagulant medications will return to the body and exacerbate bleeding risks or other side effects [11]. Achieving continuous and safe anticoagulant therapy for patients without the supervision of caregivers has become the first major challenge of wearable artificial livers. (2) The well-recognized artificial liver devices include the Molecular Adsorbent Recirculating System™ (MARS™), the

Peer review under responsibility of KeAi Communications Co., Ltd.
* Corresponding author. College of Polymer Science and Engineering, State Key Laboratory of Polymer Materials Engineering, Sichuan University, Chengdu, 610065, China.
** Corresponding author. College of Polymer Science and Engineering, State Key Laboratory of Polymer Materials Engineering, Sichuan University, Chengdu, 610065, China.
E-mail addresses: zhaoscukth@163.com (W. Zhao), zhaochsh70@163.com (C. Zhao).

https://doi.org/10.1016/j.bioactmat.2022.06.019
Received 30 March 2022; Received in revised form 25 June 2022; Accepted 27 June 2022

Abbreviation

Word	
AA	Acrylic acid
AIBN	2,2-azobisisobutyronitrile
ALB	Albumin
ALP	Alkaline phosphatase
ALT	Alanine aminotransferase
AMPS	2-acrylamido-2-methyl-1-prroanesulfonic acid
APS	Ammonium persulfate
APTT	Activated partial thromboplastin time
AST	Aspartate aminotransferase
BFbg	Bovine fibrinogen
BSA	Bovine serum albumin
$CaCl_2$	Calcium chloride
CHOL	Cholesterol
Cl	Serum chlorine
CREA	Creatinine
DBIL	Direct bilirubin
DMAC	N,N-dimethylacetamide
Eos	Eosinophils
GA	Glutaraldehyde
GGT	γ-glutamyl transpeptidase
Ghost	Cellular debris
GLB	Globulin
HCT	Hematocrit
HGB	Hemoglobin
K^+	Serum potassium
KPM	Kevlar porous microspheres
LDL-C	Low-density lipoprotein cholesterol
LiCl	Lithium chloride
Lym	Lymphocyte
MBA	*N, N′*-methylene bisacrylamide
Mon	Monocyte
Na^+	Serum sodium
NaOH	Sodium hydroxide
Neu	Neutrophil
PBS	Phosphate buffer
PES	Polyethersulfone
PLTs	Platelet
PPP	Platelet-poor plasma
PT	Prothrombin time
PVP	Polyvinylpyrrolidone
RAHMs	Reinforced anticoagulant hydrogel microspheres
RBCs	Red blood cells
rGO	Reduced graphene oxide
TBIL	Total bilirubin
TG	Triglyceride
TP	Total protein
TT	Thrombin time
UREA	Urea
VP	*N*-vinyl-2-pyrrolidone
WBCs	White blood cells

Single-Pass Albumin Dialysis system and the Fractionated Plasma Separation and Adsorption system (Prometheus™) [12]. These devices always need to separate plasma and further adsorb toxins in plasma, which extremely limits the miniaturization of artificial livers. How to realize safe and effective toxin removal in whole blood has become the second major challenge of wearable artificial livers. (3) All of the treatments or studies of wearable artificial livers should be person-centered. The design of wearable artificial liver devices should not only take into account safety and toxin removal efficiency but also consider the economic applicability of patients. Reducing the economic burden of patients has become the third major challenge of wearable artificial livers.

To solve some of the abovementioned challenges, we proposed a self-anticoagulant bilirubin adsorbent (rGO@HepMBm) to remove bilirubin from whole blood in a previous report [13]. The heparin-mimetic biomacromolecule (HepMBm) could inhibit the activities of coagulation factors VIII, IX, XI, and XII and suppress the intrinsic coagulation pathway, thus exhibiting anticoagulant activity. The introduction of reduced graphene oxide (rGO) endowed the microspheres with high bilirubin removal efficiencies. However, bilirubin is a hydrophobic lipophilic molecule that repels heparin-mimetic molecules. To improve the adsorption capacity of bilirubin, it is necessary to introduce a large amount of rGO. Unfortunately, the large amount of rGO may sacrifice the self-anticoagulant ability of the microspheres as well as increase the production cost. Although such bifunctional microspheres have both anticoagulant and toxin removal functions, they cannot maximize the two functions. Moreover, the *in vivo* safety and adsorption efficiency of rGO@HepMBm have not been verified. To achieve safe blood purification without anticoagulant medications, we designed reinforced anticoagulant hydrogel microspheres (RAHMs) in another previous report [14]. The RAHMs could bind coagulation factors in the extracorporeal circuit, thus preventing blood clotting. Importantly, RAHMs will not return to the body and be conducive to the rapid recovery of coagulation function. In healthy beagle models, the RAHMs realized 2 h blood purification without heparin. Encouragingly, the coagulation functions and the levels of coagulation factors of RAHMs-treated beagles returned to normal levels quicker than those of the heparin-treated group.

Inspired by the excellent anticoagulation of RAHMs, we proposed the "**solid anticoagulant microspheres**" to supersede water-soluble anticoagulant in the artificial liver. Solid anticoagulant microspheres can be polymer or hydrogel microspheres with excellent anticoagulant properties. To realize the idea of wearable artificial liver, we further proposed the **"anticoagulant + column"** for whole blood hemoperfusion to get rid of the plasma separation system and the heparin pump and realize the miniaturization of wearable artificial liver. The first deck of the "anticoagulant + column" is filled with solid anticoagulant microspheres, which could reduce the bleeding risks for patients and supersede the heparin pump to further reduce the weight of the wearable artificial liver. The second deck of the column could be filled with different adsorbent microspheres to adsorb different toxins. Both the anticoagulant microspheres and adsorbents should exhibit good biocompatibility for whole blood hemoperfusion.

As a proof of concept, the first deck of the column was filled with RAHMs to exhibit anticoagulant function; the second deck of the column was filled with Kevlar porous microspheres (KPMs) to remove bilirubin from whole blood. The aromatic amide polymers have strong intra- and intermolecular hydrogen bonds and π-π conjugation interactions with the benzene ring [15], so they have a strong affinity for bilirubin [16,17]. Furthermore, the KPMs could be fabricated by a simple phase inversion method, indicating that they are suitable for industrial production with low cost. In addition, we designed the principle machine of wearable artificial liver, which is lightweight (approximately 9 kg) without the plasma separation system and heparin pump unit. We anticipate that the "anticoagulant + column" and the wearable artificial liver system could provide a safe, efficient and low-cost blood purification method, which will be a milestone in the clinical development of wearable artificial livers.

2. Experimental section

2.1. Materials and reagents

Kevlar III (3 wt% polymer solution, provided by China Bluestar Chengrand Co., Ltd.). Polyethersulfone (PES, Ultrason E6020P) was obtained from BASF Chemical Company. Lithium chloride (LiCl, AR, 99.9%), bilirubin (98%), sodium hydroxide (NaOH, AR, 96%), bovine serum albumin (BSA, BR, 96%), *N*-vinyl-2-pyrrolidone (VP, 99%), acrylic acid (AA, AR, 99%), 2-acrylamido-2-methyl-1-prroanesulfonic acid (AMPS, 98%), *N, N′*-methylene bisacrylamide (MBA, 99%), 2,2-azo-bisisobutyronitrile (AIBN, 98%), ammonium persulfate (APS, 99.99%), and calcium chloride ($CaCl_2$, AR, 96%) were purchased from Aladdin Reagent Co. Ltd. Bovine fibrinogen (BFbg, 50–70% protein) was purchased from Yeasen Biotechnology Co., Ltd. N,N-dimethylacetamide (DMAC, AR, 99%), glutaraldehyde (GA, 50 wt % in water) were purchased from Chengdu Kelong Inc., China. Deionized water (DI water) was used throughout the study.

2.2. Preparation of PES microspheres and reinforced anticoagulant hydrogel microspheres (RAHMs)

PES is a commonly used material in hemodialysis, and pure PES microspheres (PESs) were prepared. First, a 16 wt% PES solution was prepared in DMAC. Then, the PES solution was dropped into DI water to form PES microspheres with a 24-gauge stainless steel needle. For RAHMs, the preparation process was described in our previous study [14] (Scheme 1). In brief, a PES and polyvinylpyrrolidone (PVP) precursor solution was prepared. Then, the PES/PVP solution was dropped into the reaction solution directly by electrospray to form microspheres. The composition of the precursor solution and reaction solution is shown in Table S1. The received microspheres were heated to finish the polymerization, and the RAHMs were then obtained. The detailed experiment is recorded in the Supporting Information.

2.3. Preparation of the KPMs

The KPM precursor solution (1 wt%) was prepared by diluting the 3 wt% Kevlar III polymer solution. In brief, 40.5 g 3 wt% Kevlar III polymer solution, 75 g DMAC and 6 g LiCl were added to a beaker and stirred vigorously to obtain a homogeneous solution. As shown in Scheme 1, the KPMs were obtained by liquid–liquid phase inversion. The KPM precursor solution (1 wt%) was dropped into a 30% ethanol solution with a 23-gauge stainless steel needle. After solidification for 2 h, the KPMs were filtered and washed in DI water to remove the residual solvent thoroughly.

2.4. Characterization of the microspheres

The chemical structures of the KPMs were characterized by ATR-IR (Thermo Scientific Nicolet iS50, America) and X-ray photoelectron spectroscopy (XPS, XSAM800, Kratos Analytical, U.K.). For ATR–IR, the microspheres were completely dried and pressed into slices to obtain the FTIR spectra between 600 and 4000 cm^{-1}. For XPS, the microspheres were also dried and pressed into slices for testing. The microstructures of the KPMs were obtained by scanning cryo-electron microscopy (Apreo S HiVoc, Thermo Fisher Scientific (FEI)). To prepare the samples for cryo-SEM, the KPMs were coated with a liquid conductive adhesive and put into a box with liquid nitrogen. After 5 min, the KPMs were cut off and then observed. The thermal stability of the KPMs was characterized by thermogravimetric analysis (TGA, Mettlle Toledo, TGA/DSC 3+, Switzerland). The curves of derivative thermogravimetric (DTG) were derived from TGA data. The mechanical properties of the KPMs were investigated by a universal testing machine (SANS CMT4000, MTS). The water uptake ratio of KPMs was calculated according to the following formula (1) [18]:

$$\mathrm{WUR}\ (\%) = \frac{(W_e - W_d)}{W_d} \times 100\% \quad (1)$$

where W_e is the weight of the wet beads and W_d is the weight of the dry beads. Three parallel samples were employed, and the results are expressed as the mean ± SD (n = 3).

2.5. Evaluation of the biocompatibility of the microspheres in vitro

The biocompatibility of the microspheres *in vitro* was evaluated by hemocompatibility and cytocompatibility. For hemocompatibility, healthy human fresh blood was collected using vacuum tubes. Sodium citrate anticoagulated blood was used for clotting time tests (blue vacuum blood collection tube). After coculture with the microspheres, the blood was tested by an automated hematology cell analyzer (BC-5100, Mindray Bio-Medical Electronics Co., Ltd., Shenzhen, China). Ethylene diamine tetraacetic acid anticoagulated blood was used for evaluation of routine blood tests (purple vacuum blood collection tube), the blood was centrifuged at 4000 rpm for 15 min to obtain platelet-poor plasma (PPP), the obtained PPP was cocultured with the microspheres, and the plasma was tested by a semiautomatic blood coagulation analyzer (CA-530, Sysmex Corporation, Kobe, Japan). Hirudin anticoagulated blood was used for complement activation (red vacuum blood collection tube, 77 μL recombinant hirudin solution was added to 3 mL whole blood). After coculture with the microspheres, the generated complement factors in plasma were tested by enzyme-linked immunosorbent assay. Blood from the same donor was used throughout one kind of blood test. The experimental details for the blood compatibility of the microspheres are recorded in the Supporting Information. For cytocompatibility, the L929 fibroblast cell line was seeded in 24-well tissue culture polystyrene

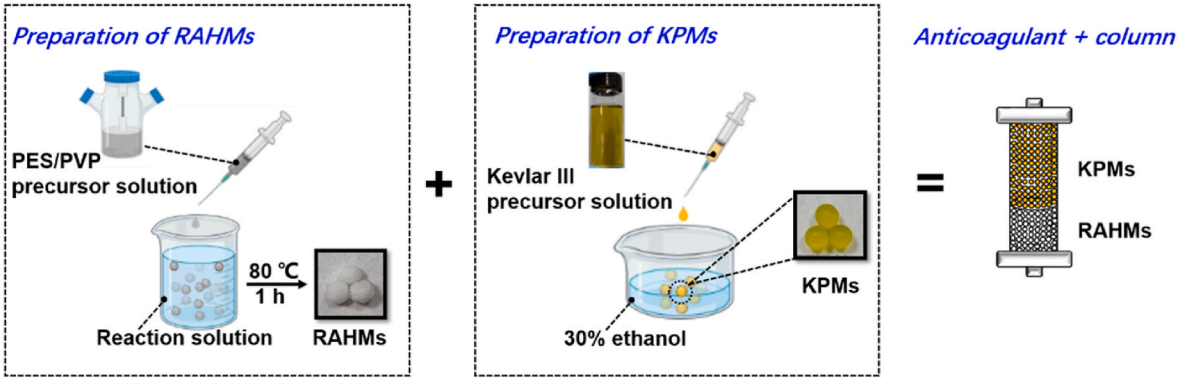

Scheme 1. Schematic illustration of the preparation of the RAHMs, KPMs and double-deck column.

plates at a density of 2.5×10^4 cells per cm^2. After coculturing for 24 h, CCK-8 (final dilution: 1:10) was used to test the cell viability. The experimental details for blood compatibility and cell viability are recorded in the Supporting Information.

2.6. Bilirubin adsorption in vitro

2.6.1. Adsorption kinetics in PBS

Bilirubin molecules are light-sensitive, so adsorption experiments should be carried out in the dark. First, a small quantity of 0.1 mol/L NaOH solution was used to dissolve bilirubin, and then the dissolved bilirubin solution was diluted with phosphate buffer solution (PBS, pH = 7.4). To study the adsorption kinetics of KPMs, 10 microspheres were added to the bilirubin solution (200 mg/L, 10 mL), and the mixture was shaken at a speed of 200 rpm in an incubator at 37 °C. The OD_{437} of the bilirubin solution was measured at 0, 30, 60, 90, and 120 min, and the adsorption amounts (q, mg/g) were calculated according to the following formula (2):

$$q = \frac{(C_0 - C_t) \times V}{m} \tag{2}$$

where C_0 is the initial concentration of bilirubin, C_t (mg/L) is the concentration of bilirubin at time t, V (mL) is the volume of the mixture solution, and m (g) is the dry weight of the samples. Three parallel samples were employed, and the results are expressed as the mean ± SD (n = 3).

Pseudofirst-order and pseudosecond-order kinetic models were used to analyze the bilirubin adsorption kinetics process. The calculation formulas are shown in formulas (3) and (4) [19]:

Pseudo first-order kinetic models:

$$ln(q_e - q_t) = lnq_e - k_1 t \tag{3}$$

Pseudo second-order kinetic models:

$$\frac{t}{q_t} = \frac{1}{k_2 q_e^2} + \frac{t}{q_e} \tag{4}$$

where q_e and q_t are the calculated saturation capacity and practical adsorption capacity, respectively. t is the adsorption time. k_1 and k_2 are the related ratio constants of the pseudo first-order and pseudo second-order kinetic models, respectively.

2.6.2. Static bilirubin adsorption at different initial concentrations

To study the effects of the concentrations on the adsorption behavior, different initial concentrations of bilirubin were prepared (100, 200, 300, 400 and 500 mg/L). Then, 10 microspheres were added to the bilirubin solution (10 mL), and the mixture was shaken at a speed of 200 rpm in an incubator (37 °C, 2 h). The OD_{437} of the bilirubin solution was measured at 2 h, and the adsorption amounts were calculated according to formula (1). Three parallel samples were applied to obtain a reliable value, and the results are expressed as the mean ± SD (n = 3).

2.6.3. Adsorption in simulated serum

Albumin is an important carrier of bilirubin in blood, and the presence of albumin might decrease the bilirubin adsorption amounts of adsorbents. Therefore, the bilirubin adsorption capacity of KPMs was evaluated in a BSA-rich solution. In brief, the concentrations of BSA and bilirubin were 10 g/L and 200 mg/L, respectively. Ten microspheres of each sample were added to the bilirubin/BSA solution, and the mixture was shaken at a speed of 200 rpm in an incubator (37 °C). Then, the OD_{437} values of the bilirubin solution were measured at 0, 30, 60, 90, and 120 min, and the adsorption amounts were calculated as mentioned above. Three parallel samples were applied to obtain a reliable value, and the results are expressed as the mean ± SD (n = 3).

2.7. Therapeutic efficacy and safety in hyperbilirubinemia beagles

2.7.1. Animal welfare

The procedures involving the use of animals in this study were prospectively reviewed and approved by the Institutional Animal Care and Use Committee. This study was conducted in accordance with the National Institutes of Health Guide for the Care and Use of Laboratory Animals (NIH Publications No. 8023, revised 1978). The experiments conformed to the legal requirements in China and were approved by the ethical committee (No. 2021911A) of West China Hospital, Sichuan University. During the experimental period, the animals had free access to water and food.

2.7.2. Establishment of hyperbilirubinemia beagle models

This study was performed on 3 healthy beagle dogs aged approximately 1–2 years and weighing approximately 10 kg. Beagles were given 3% pentobarbital sodium 30 mg/kg intramuscular anesthesia. Before the operation, blood was collected from the subcutaneous vein of the medial forelimb, and the blood biochemistry was tested. First, the abdomen was barbered and disinfected. Then, the abdominal skin was sliced open with an electrosurgical knife. The gallbladder and common bile duct were found under the liver, and the bile duct was separated. After confirmation of bile outflow, the bile duct was ligated with a double ligation, and the abdomen was closed. Blood samples were collected to monitor the bilirubin concentration every two days after the operation. Approximately 7 days later, the total bilirubin concentration increased to approximately 100 μmol/L.

2.7.3. Hemoperfusion therapy

We used a principle machine of wearable artificial liver (Chengdu Ruierkewei Co., Ltd., China) and extracorporeal circulation blood tubes (Chengdu OCI Medical Devices Co., Ltd., China) to perform hemoperfusion. The total blood on the extracorporeal circulation tubes was approximately 100 mL, which included the volumes of the extracorporeal circulation blood tube (80 mL) and hemoperfusion column (20 mL). The design drawing of the hemoperfusion column is shown in Fig. S9. Before the treatment, the extracorporeal circulation blood tubes were pre-rinsed with normal saline and heparin-containing saline until there was no residual air. The dog was weighed and anesthetized with 3% pentobarbital sodium (30 mg/kg, intramuscular injection). Then, the femoral vein was isolated, punctured and fixed with a two-lumen catheter (GDK-612.5P, Gambro Kathetertechnik Hechingen, Germany), which was connected to the extracorporeal circulation blood tubes. Before hemoperfusion treatment, 625 IU (0.5 mL, 1250 IU/mL) heparin was pre-injected into the dog. Five minutes later, hemoperfusion was performed with a blood flow rate of 60 mL/min and treated for 3 h. During the 3 h treatment, no extra heparin was used. Blood samples were drawn from the extracorporeal circulation blood tubes at 0, 15, 30, 45, 60, 90, 120 and 180 min. To reduce the blood loss of dogs, normal saline was used to return blood to the dog at the end of the treatment. After the experiments, the operative wounds of the dogs were carefully sutured, and the dogs were executed. The blood count assays, blood biochemistry and clotting times of the collected blood samples were performed by West China-Frontier Pharma Tech Co., Ltd. The experiments were repeated three times to obtain reliable results, and the results are expressed as the mean ± SD (n = 3).

2.8. Statistical analysis

Each experiment was performed independently and quantified in at least triplicate. The results are presented as the mean ± standard deviation. Statistical significance was determined by two-tailed Student's t tests for two groups and one-way ANOVA for multiple groups, and $p < 0.05$, $p < 0.01$ and $p < 0.001$ were considered significant differences (marked with *, ** and ***, respectively).

3. Results and discussion

3.1. Characterization of the microspheres

The FTIR spectra of RAHMs are shown in Fig. S1. The peak at 3384 cm^{-1} was attributed to the O–H bond in PAA. The peak at 1639 cm^{-1} was attributed to the –C═O stretching vibration in PVP and PAA, indicating that PVP was successfully introduced into the RAHMs. The characteristic peak of AMPS was at 1045 cm^{-1}, which was ascribed to the S–O stretching vibration of the $–SO_3$ group. The surface and cross-sectional images of the RAHMs are shown in Fig. S2. The surface was rough and corrugated, which was due to the introduction of hydrogel. For the cross-sectional morphology of the RAHMs, a porous structure was observed. Similar results were obtained in a previous report [14], which suggested the successful preparation of RAHMs.

Kevlar is a well-known para-aramid fiber that is famous for its ultra-strong mechanical properties and resistance to chemical attack [20]. Kevalar III is synthesized by p-phenylenediamine, terephthaloyl

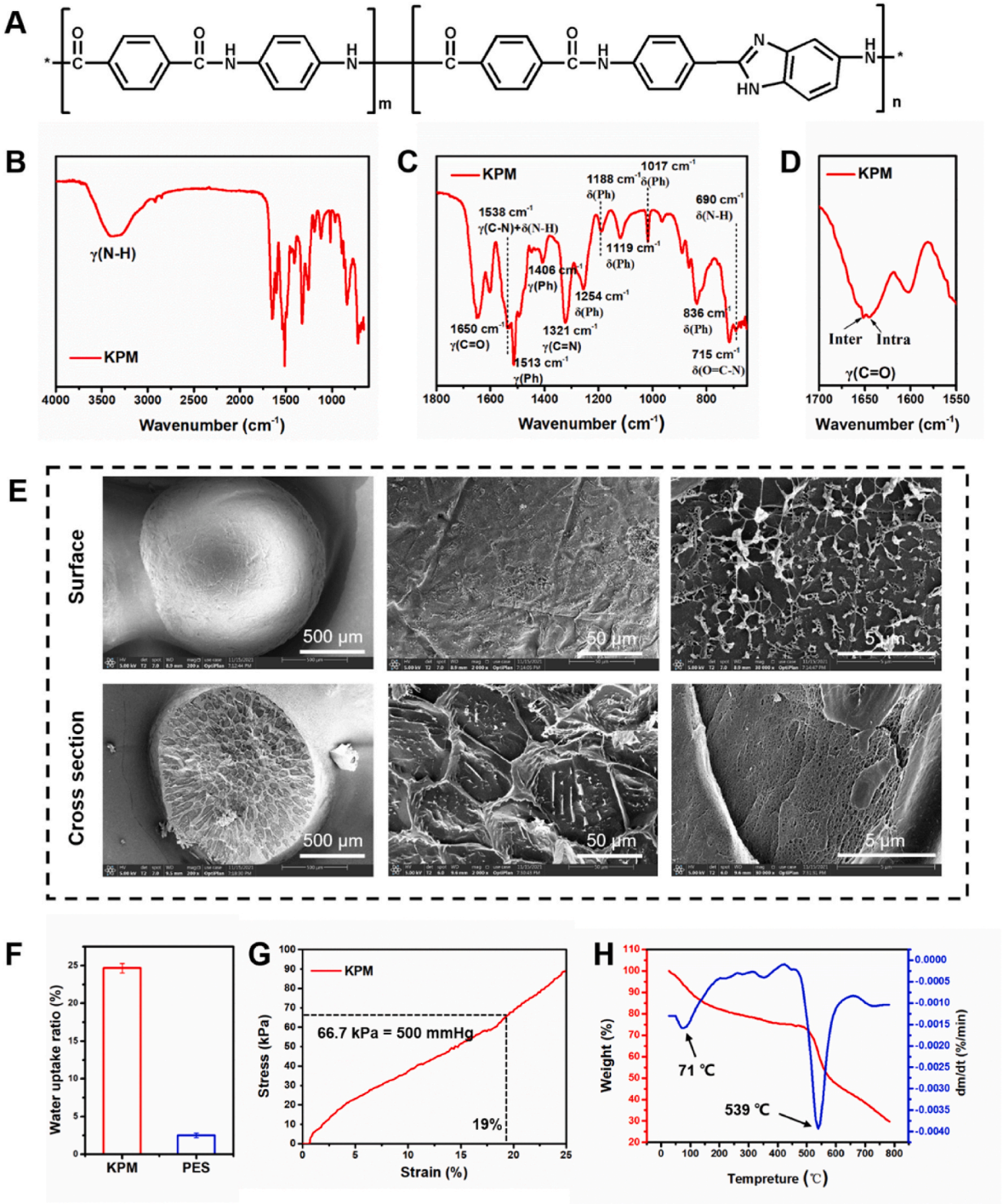

Fig. 1. Physicochemical characterization of the microspheres. (A) Structural formula of Kevlar III. (B–D) FTIR spectra for KPMs. γ and δ represent the stretching and bending modes of different functional groups, respectively. (E) The surface and cross-sectional images of KPMs were obtained by scanning cryo-electron microscopy at different magnifications. The magnifications of these photos were 200 × , 2000 × , 30000 × from left to right. (F) Water adsorption of the PESs and KPMs in normal saline (n = 3). (G) Typical compressive stress–strain curves of KPMs. (H) The TGA and DTG curves of KPMs.

chloride and 2-(4-aminophenyl)-1H-benzimidazol-5-amine. The introduction of heterocyclic monomers reduces the regularity and crystallinity of the polymer chains and forms stronger intermolecular hydrogen bonds than Kevlar fibers [21]. Therefore, the Kevalar III fiber has high strength, high modulus and high elongation at break. The structural formula of Kevlar III is shown in Fig. 1A. Owing to the strong intermolecular hydrogen bonds, the pure polymer has a strong affinity for bilirubin. Moreover, it can be dropped into microspheres by a simple phase inversion method, as shown in Scheme 1. The chemical construction of the prepared Kevlar III porous microspheres (KPMs) was confirmed by FTIR. The peaks were similar to the reported results [15]. As Fig. 1B and C shows, the peaks at 3350 and 1650 cm^{-1} were attributed to the N–H stretching vibration and C═O stretching vibration of amide groups, respectively. The peaks at 1513 and 836 cm^{-1} were attributed to the C═C stretching vibration and C–H stretching vibration of the aromatic ring, respectively. The peak at 1321 cm^{-1} was attributed to the C═N stretching vibration of the heteroaromatic ring. These results indicated the structure of aromatic amides. Of note, two peaks were split at the C═O vibration mode (Fig. 1D), which was attributed to intra- and inter-hydrogen bonds [15]. The XPS survey scan spectra are shown in Fig. S3, and the C 1s, N 1s, and O 1s signals of the KPMs were clearly observed. In the XPS spectrum of C 1s (Fig. S3B), the peaks at 284.7 eV and 287.7 eV were assigned to the C═C bond of the aromatic ring and the C═O bond of the amide groups, respectively. In the XPS spectrum of N 1s (Fig. S3C), the peaks at 396.7 eV and 395.0 eV were assigned to the N–H bond of amide groups and the C═N bond of heteroaromatic rings, respectively. In the XPS spectrum of O 1s (Fig. S3D), the peak at 582.6 eV was assigned to the C═O bond of amide groups, and these results indicated that the heteroaromatic ring was successfully introduced.

The surface and cross-sectional images of KPMs are shown in Fig. 1E. The KPMs showed spherical and smooth surfaces with a diameter of approximately 1–2 mm. Furthermore, the surface of KPMs showed entangled nanofiber networks. In the cross-sectional images of KPMs, abundant macropores and mesopores were observed. The size of the macropores was 73.2 ± 29.5 μm, which was measured by Image J (Fig. S4). To evaluate the pore size distribution and specific surface area in the microspheres more accurately, a mercury injection apparatus was used. As Fig. S5 and Table S2 show, the pore size was mainly distributed from 500 to 5000 nm, the pore volume of the KPMs was 7.3 mL/g, and the specific surface area was 22.7 m^2/g. These pores were generated by solvent exchange, and entangled nanofibers were formed owing to the strong hydrogen bonding interactions. Owing to the porous structure and strong hydrogen bonding interactions, the KPMs exhibited a higher water uptake ratio (24.7 g/g) than the PESs (2.5 g/g) (Fig. 1F). The high water uptake ratio of KPMs could accelerate the diffusion of toxin and improve the adsorption capacity.

Adsorbent materials should be able to withstand 100–500 mmHg blood hydrodynamic pressure, as shown in Fig. 1G. The KPMs exhibited strong compressive capacity, and the strain of KPMs was 19% at 500 mmHg, which indicated that they would not be broken under high blood pressure. The thermostability of the KPMs was determined by TGA and DTG (Fig. 1H). Two peaks at 71 °C and 539 °C were observed in the DTG curves, which could be ascribed to the evaporation of H_2O and the degradation of the Kevlar III skeleton, respectively. These results indicated that the KPMs had high thermostability for transportation and hemoperfusion treatment. Overall, the KPMs are electroneutral and porous and can be powerful candidates for hemoperfusion adsorbents.

3.2. Biocompatibility of the KPMs in vitro

3.2.1. Hemolysis ratios

Since erythrocytes are the most abundant cells in blood, abnormal/broken erythrocytes may lead to hemolytic jaundice, hemolytic anemia and renal dysfunction [22]. The hemolysis ratio is an important indicator to evaluate the hemocompatibility of blood-contacting materials. The hemolysis ratio of RAHMs was less than 1% in a previous report [14]. As Fig. 2A shows, the hemolysis ratios of the PESs and KPMs were less than 5%, which is safe for clinical use according to the American Society for Testing and Materials (ASTM) standard (ASTM F756−2008). Furthermore, no obvious broken erythrocytes were observed after contact with the microspheres (Fig. 2B).

3.2.2. Routine blood tests

The activation of leukocytes and platelets may cause complement activation, inflammatory factor release and thrombosis [23,24]. Routine blood tests are the cornerstone to evaluate the hemocompatibility of biomaterials. The RAHMs had no distinct influence on the blood cell count in a previous report [14]. For PESs and KPMs, the blood cell counts of whole blood were measured after coculturing with the microspheres for 1 h. As Fig. 2C shows, the levels of white blood cells (WBCs), red blood cells (RBCs), and platelets (PLTs) showed no distinct changes after contact with the PESs and KPMs (Fig. 2C (i)). The levels of hemoglobin (HGB) were not significantly different among these groups, while the levels of hematocrit (HCT) increased slightly after contact with the PESs and KPMs (Fig. 2C (ii)), which may be due to water evaporation during coculturing. Moreover, the distribution of white blood cells revealed the activation of the complement system and immune system, as shown in Fig. 2C (iii). Whole blood had no significant change in leukocyte differential count after contact with the PESs and KPMs. The detailed data are recorded in Table S3.

3.2.3. Complement activation

The complement system is a rapid and efficient immune surveillance system. It is the first line of defense against microbial intruders [25]. Human complement fragments 3a (C3a) and 5a (C5a) are often chosen as indicators to evaluate the activation of the complement system, since they are protein fragments released during complement activation [26]. The RAHMs exhibited inhibitory effects on complement activation in a previous report [14]. For the generated C3a, the PESs and KPMs showed no significant difference compared to the negative control (Fig. 2D). Moreover, the generated C5a of the PESs and KPMs was significantly decreased compared with that of the negative control (Fig. 2E). The results indicated that PESs and KPMs do not activate the complement system and cause inflammation.

3.2.4. Clotting times

The anticoagulation properties of the RAHMs were systematically evaluated by Song et al. [14]. In brief, the activated partial thromboplastin time (APTT) and thrombin time (TT) of plasma after incubation with RAHMs exhibited a notable dose-related prolongation, but the prothrombin time (PT) of plasma after incubation with RAHMs showed no significant difference compared to that of platelet-poor plasma (PPP). Moreover, the RAHMs showed inhibitory effects on coagulation factors (especially factor VIII), which suggested that the RAHMs could inhibit the intrinsic coagulation pathway to exert anticoagulation properties.

The KPMs were electroneutral and had no effect on the blood acid-base electrolyte balance. The plasma was cocultured with the PESs and KPMs for 30 min, and then the APTT, TT and PT of the plasma were measured. As Fig. 2F shows, the APTT, TT and PT of the plasma showed no significant change after coculturing with the PESs and KPMs, which suggested that the KPMs had no significant influence on the coagulation system.

3.2.5. Cytocompatibility

The RAHMs showed no obvious cytotoxicity, as reported by Song et al. [14]. The PESs and KPMs showed good cytocompatibility with L929 cells *in vitro*, the cell viability of the PESs and KPMs was maintained at approximately 100% (Fig. 2G), and live/dead staining (Fig. S6) further confirmed the good cytocompatibility of the microspheres.

3.2.6. Protein adsorption

Albumin is the carrier of bilirubin in blood circulation [27]. The

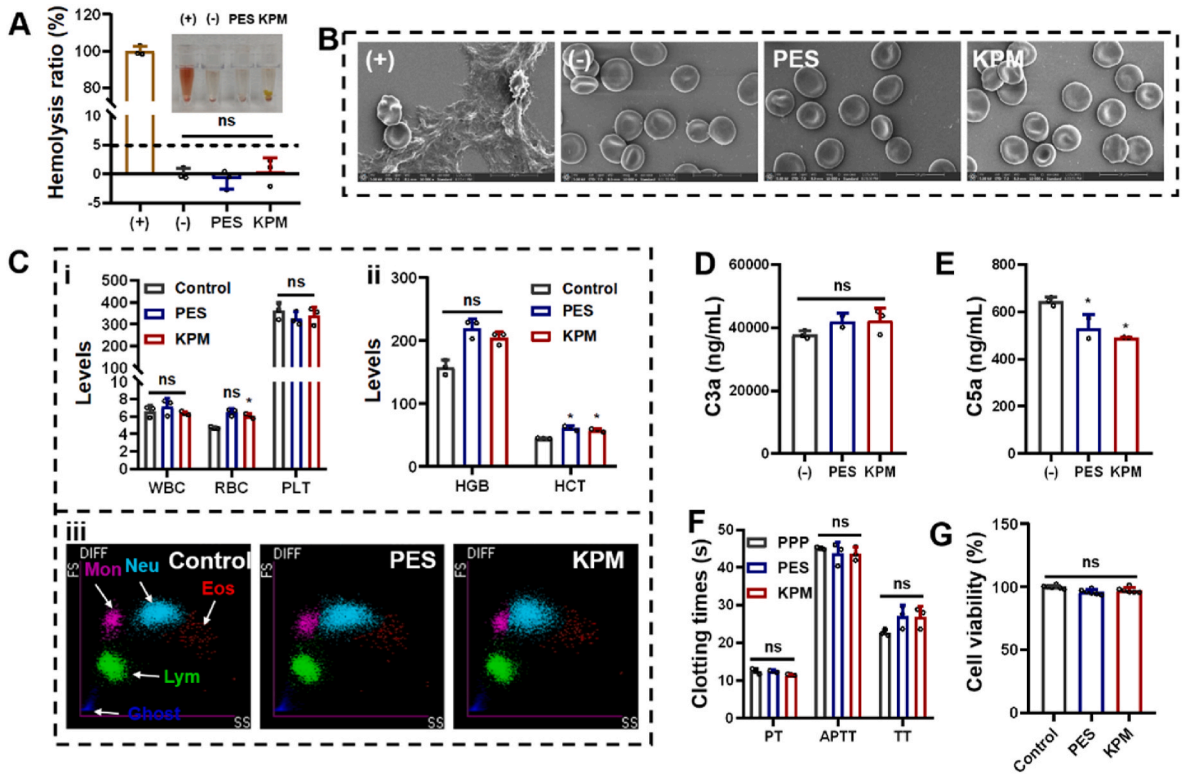

Fig. 2. Evaluation of the biocompatibility of microspheres *in vitro*. (A) Hemolysis ratio and digital photos of the samples (n = 3). The negative control was normal saline, and the positive control was deionized water. (B) SEM images of RBCs after contact with the microspheres. (C) Routine blood tests of whole blood after coculturing with microspheres for 1 h (n = 3). (i) Levels of main blood cells, (ii) levels of HGB and HCT, (iii) differential white blood cell count (DIFF) scatter (forward (FS), side (SS)) charts of blood after coculturing with the microspheres. The control group was whole blood. (D, E) The generated C3a and C5a in blood after coculturing with microspheres for 1 h. The results were measured by ELISAs (n = 3). The negative control was whole blood. (F) Clotting times of PPP after coculturing with microspheres for 30 min (n = 3). (G) Cell viability of the PESs and KPMs cocultured with L929 cells for 24 h. The results were measured by CCK8 assay (n = 6). PPP: platelet-poor plasma, WBC: White blood cells, RBC: red blood cells, PLT: platelets, HGB: hemoglobin, HCT: hematocrit, Mon: monocyte, Neu: neutrophil, Eos: eosinophils, Lym: lymphocyte, Ghost: cellular debris. PT: prothrombin time, APTT: activated partial thromboplastin time, TT: thrombin time.

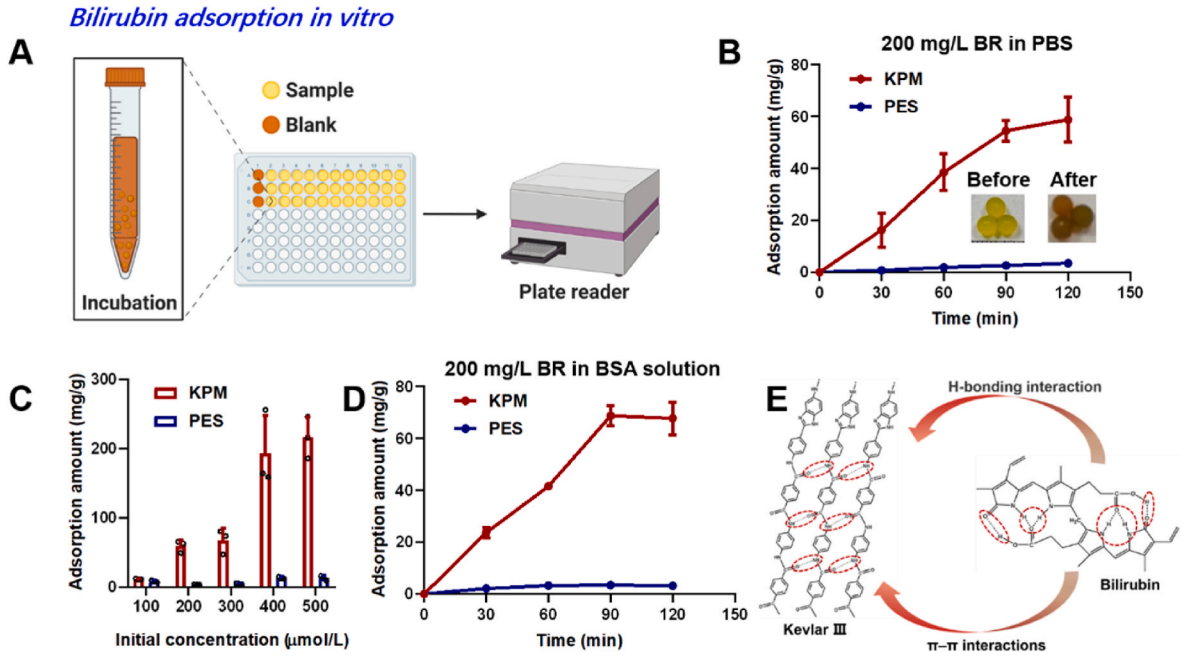

Fig. 3. Bilirubin adsorption *in vitro*. Ten microspheres were immersed in 10 mL bilirubin solution, and the OD_{437} was measured by a plate reader at different time points. (A) Schematically illustrating the bilirubin adsorption experiment. (B) Bilirubin adsorption kinetics of KPMs (T = 37 °C, initial bilirubin = 200 mg/L), (n = 3). (C) Adsorption ability of KPMs at different initial concentrations (T = 37 °C, t = 2 h), (n = 3). (D) Bilirubin adsorption in simulated serum (T = 37 °C, initial bilirubin = 200 mg/L, BSA = 10 g/L) (n = 3). (E) Adsorption mechanism of KPMs.

affinity of the adsorbent to albumin may facilitate the adsorption of bilirubin. In addition, Fbg is an important protein involved in coagulation and hemostasis. Therefore, the adsorption capacity of KPMs for BSA and BFbg was investigated. As Fig. S7 shows, the adsorption amounts of RAHMs and KPMs for BSA were 14.8 and 38.4 μg/g, respectively, which indicated that the KPMs might have affinity for BSA and a higher affinity for bilirubin than RAHMs. Similarly, the adsorption amounts of RAHMs and KPMs for BFbg were 15.5 and 24.0 μg/g, respectively, which indicated that the KPMs might adsorb protein in serum. Since bilirubin molecules are lipophilic and hydrophobic, the adsorbents that have affinity for bilirubin must also have affinity for plasma proteins.

Overall, these results indicated that the KPMs exhibited good biocompatibility and high affinity to proteins, which might facilitate the adsorption of bilirubin in whole blood perfusion.

3.3. Bilirubin adsorption in vitro

The bilirubin adsorption method is shown in Fig. 3A. KPMs were immersed in bilirubin solution, and blank samples without KPMs were also prepared. The OD_{437} was tested by a plate reader, and the adsorption amount was calculated after subtracting the amount of decomposed bilirubin.

3.3.1. Adsorption kinetics

To study the adsorption kinetics, the time-dependent adsorption amounts were measured. As Fig. 3B shows, the bilirubin adsorption amounts of KPMs increased dramatically in the first 90 min, while the bilirubin adsorption amounts of the PESs increased slowly. After 90 min, the adsorption rates decreased, and the adsorption gradually reached equilibrium at 120 min. The maximum adsorption amounts of the KPMs and PESs were 58.9 mg/g and 3.5 mg/g, respectively. The outstanding adsorption performance of the KPMs was driven by hydrogen bonds and π−π interactions with bilirubin (Fig. 3E). Furthermore, the abundant macropores (Fig. S5 and Table S2) also facilitate the adsorption of bilirubin.

The adsorption mechanism was studied by two kinds of kinetic models. The pseudo first-order equation (Lagergrenrate equation) is the first rate equation for the liquid–solid system based on a solid adsorbent. The pseudo second-order equation is based on the assumption that adsorption rates are controlled by chemisorption mechanisms, and the adsorption process involves electron transfer between adsorbents and adsorbed substances. As Fig. S8 and Table S4 show, the correlation coefficient values (r_1^2) of bilirubin adsorption for KPMs and PESs were 0.96 and 0.99, respectively. On the other hand, the correlation coefficient values (r_2^2) of bilirubin adsorption for KPMs and PESs were 0.96 and 0.05, respectively. Moreover, the calculated $q_e(q_{e(cal)})$ values in the pseudo first-order equation for the KPMs and PESs were 83.0 and 4.8 mg/g, respectively, while the $q_e(q_{e(cal)})$ values in the pseudo second-order equation of KPMs and PESs were 54.3 and 24.6 mg/g, respectively. These results indicated that the adsorption process of KPMs agreed well with the pseudo first-order equation.

3.3.2. Adsorption ability at different initial concentrations

The initial concentration was an important influencing factor on the adsorption behavior. As Fig. 3C shows, the adsorption amounts of KPMs increased with increasing bilirubin concentration. The adsorption amounts of KPMs were 11.3, 58.9, 67.1, 193.1, and 216.1 mg/g in the 100, 200, 300, 400, and 500 mg/L bilirubin solutions, respectively. However, the adsorption amounts of PESs were not significantly increased. The bilirubin concentration of clinical hyperbilirubinemia patients is often higher than 200 mg/L, and the KPMs possessed a higher adsorption capacity with the higher initial bilirubin solution. The results indicated that the KPMs could be an effective adsorbent for hyperbilirubinemia patients.

3.3.3. Adsorption in simulated serum

Albumin is a bilirubin carrier in blood, and there are many binding sites on albumin to bind bilirubin [28]. The presence of albumin might significantly inhibit bilirubin adsorption during hemoperfusion therapy. The bilirubin/BSA solution was prepared to simulate the plasma environment and evaluate the bilirubin adsorption capacity. As Fig. 3D shows, the bilirubin adsorption amount of KPMs in BSA-rich solution was approximately 67.8 mg/g, which was higher than the adsorption amount of KPMs in PBS. For most bilirubin adsorbents, the bilirubin adsorption capacity in BSA-rich solution was lower than that in PBS owing to their resistance to BSA. In this work, the excellent adsorption capacity of KPMs was driven by the strong van der Waals force between KPMs and BSA (Fig. 3E).

3.4. Therapeutic efficacy and biosafety in beagles with hyperbilirubinemia

3.4.1. Toxin removal efficiency

The body weights and sexes of the dogs are recorded in Table S5. Hyperbilirubinemia beagle models were established by bile duct ligation [29] (Fig. 4A). Approximately 7 days later, as shown in Fig. 4B, the concentrations of total bilirubin (TBIL) and direct bilirubin (DBIL) increased significantly from 0.7 to 0.5 to 135.2 and 119.6 μmol/L, respectively. Meanwhile, alanine aminotransferase (ALT), aspartate aminotransferase (AST), alkaline phosphatase (ALP) and γ-glutamyl transpeptidase (GGT) increased significantly from 28.7, 23.9, 58.2 and 1.2 to 469.7, 59.7, 1137.7 and 50.7 U/L, respectively. These results indicated that cholestatic hyperbilirubinemia was successfully established.

The hemoperfusion process is shown in Fig. 4C and D. Before hemoperfusion therapy, the hyperbilirubinemia beagle was anesthetized and strapped. Then, the femoral vein was isolated, punctured and fixed with a two-lumen catheter to provide blood access. Heparin (625 IU, 0.5 mL, 1250 IU/mL) was intravenously injected into the dog, and 5 min later, hemoperfusion was initiated. The blood passed through the RAHMs first to prevent coagulation. Then, the blood passed through the KPMs to remove bilirubin. During the 3 h hemoperfusion, no extra heparin was used. As Fig. 4E shows, the concentrations of TBIL and DBIL substantially decreased during the first 1 h of hemoperfusion; then, the adsorption capacity of KPMs reached saturation, and the concentrations of TBIL and DBIL remained the same. The concentrations of TBIL and DBIL were decreased from 153.6 to 139.1 to 105.5 and 97.7 μmol/L, respectively. The removal efficiencies of KPMs to TBIL and DBIL were 31.4% and 29.2%, respectively. The saturated adsorption capacity of KPMs in hyperbilirubinemia beagles' whole blood hemoperfusion was 213.8 μmol/L KPMs (we assume that the average dog weight is 10 kg and their average circulating blood volume is 8% of body weight). Meanwhile, the concentrations of ALP, ALT, AST and GGT also decreased significantly, and the removal efficiencies of ALP, ALT, AST and GGT were 24.9%, 32.0%, 19.8%, and 27.5%, respectively. The decrease in ALP, ALT, AST and GGT might be due to hydrogen bonds with the KPMs, since the ALP, ALT, AST and GGT are also proteins. Moreover, the body temperatures of the dogs showed no obvious change during the hemoperfusion treatment (Fig. 4G), which indicated that no infection or inflammatory response occurred. These results indicated that the KPMs could not only remove bilirubin from whole blood but also reduce liver damage and improve clinical outcomes.

3.4.2. Anticoagulant performance of the anticoagulant + column

This is the first trial of an artificial liver to perform without systemic heparinization treatment in hyperbilirubinemia beagle models. In clinical hemoperfusion, the initial dose of heparin should be 50 IU/kg, and 937.5 IU/h of heparin needs to be appropriately added according to vascular access and transmembrane pressure, and a total of 2875 IU heparin is required for a 10 kg beagle in 3 h hemoperfusion. In this work, only 1125 IU heparin was used (625 IU pre-injected and 500 IU in extracorporeal circulation blood tubes). Compared with clinical

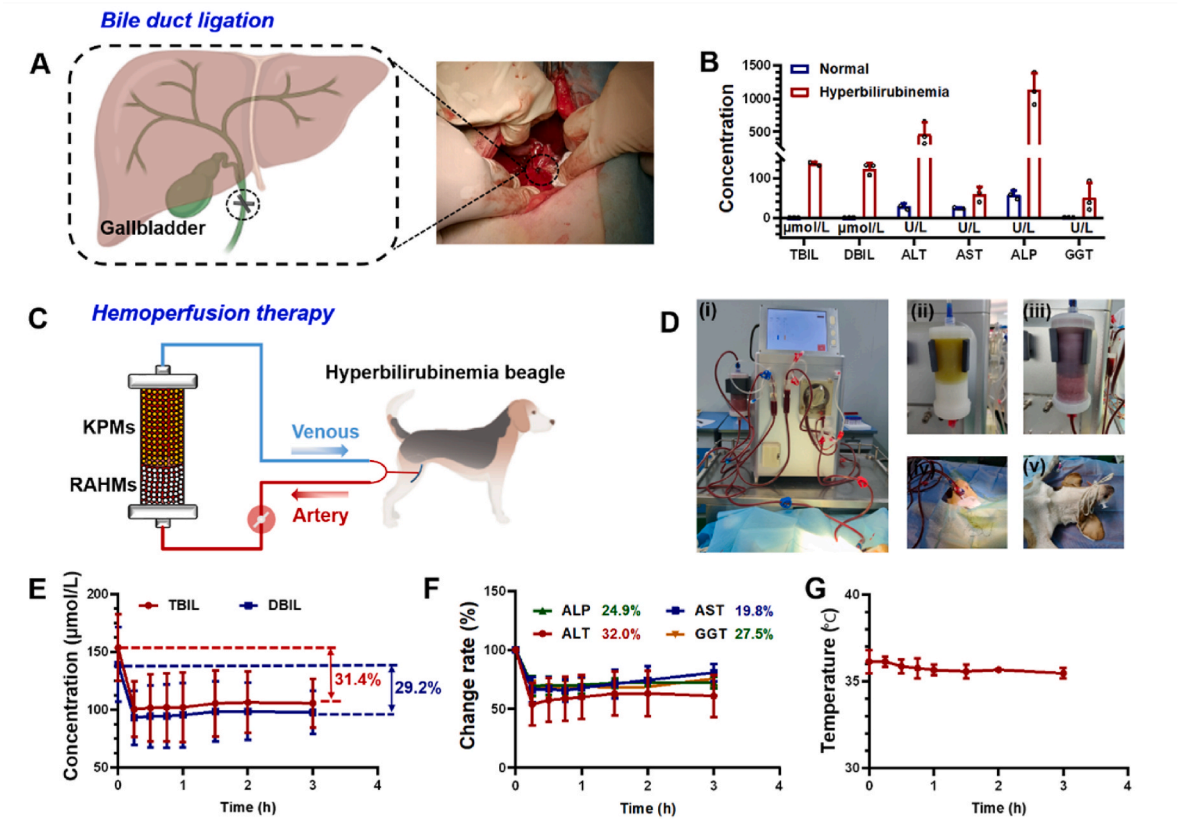

Fig. 4. Hemoperfusion therapy in hyperbilirubinemia beagle models. (A) Bile duct ligation to establish hyperbilirubinemia beagle models. (B) The main indicators of liver function between normal and hyperbilirubinemia beagles (n = 3). (C) Schematically illustrating hemoperfusion therapy and the circulation direction. (D) Photos during hemoperfusion therapy: (i) the working hemoperfusion machine; (ii) the double-deck column before the blood flowed and its orientation; (iii) the double-deck column after the blood flowed; (iv) the venipuncture site with a two-lumen catheter to provide blood access; (v) the hyperbilirubinemia beagle was strapped and anesthetized with 3% pentobarbital sodium (30 mg/kg, intramuscular injection). (E) The concentrations of TBIL and DBIL during hemoperfusion therapy (n = 3). (F) The main indicators of liver function during hemoperfusion therapy (n = 3). (G) The body temperatures of dogs during 3 h of hemoperfusion treatment (n = 3). TBIL: total bilirubin, DBIL: direct bilirubin, ALT: alanine aminotransferase, AST: aspartate aminotransferase, ALP: alkaline phosphatase, GGT: γ-glutamyl transpeptidase.

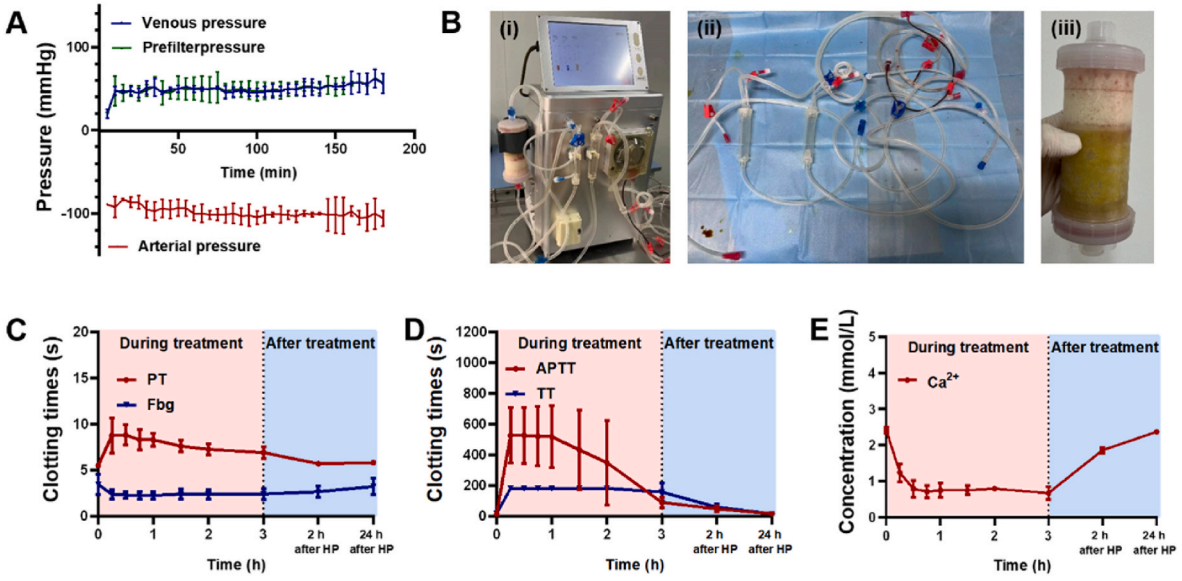

Fig. 5. Anticoagulant performance of the **"anticoagulant + column"** without systemic heparinization treatment in whole blood hemoperfusion. (A) The pressure changes of the hemoperfusion machine during 3 h of hemoperfusion treatment (n = 3). (B) Photos of the hemoperfusion machine (i), extracorporeal circulation blood tubes (ii), and double-deck column (iii) after returning blood to normal saline. (C) PT and Fbg of the dogs at different time intervals (n = 3). (D) APTT and TT of the dogs at different time intervals (n = 3). (E) The concentrations of serum calcium at different time intervals (n = 3). PT: prothrombin time, Fbg: fibrinogen, APTT: activated partial thromboplastin time, TT: thrombin time. The detection upper limits of APTT and TT were 600 s and 180 s, respectively.

systemic heparinization treatment, approximately 60% heparin was reduced with 120 mL solid anticoagulant microspheres.

To monitor the coagulation functions of the dogs, the pressure changes of the hemoperfusion machine were recorded, and blood samples were collected at different time intervals. As Fig. 5A shows, the venous pressures, arterial pressures and prefilterpressures were within the range of normal fluctuations, which indicated that there was no thrombus in the extracorporeal circulation blood tubes. Furthermore, normal saline was used to return blood to the dog at the end of treatment, and there was no thrombus observed in the extracorporeal circulation blood tubes or the "anticoagulant + column" (Fig. 5B). As Fig. 5C shows, during the 3 h hemoperfusion, the levels of Fbg were monotonous, while the clotting times of PT increased slightly. However, APTT and TT showed dramatic prolongation (Fig. 5D). The results were similar to our previous study [14], which showed that the heparin-treated dogs had significant prolongation of APTT and TT. For APTT, the prolongation gradually decreased and returned to 89.3 s after 3 h of hemoperfusion (the APTT of the healthy dogs was approximately 12.4 s), which indicated that the "anticoagulant + column" could surpport at least 3 h hemoperfusion. Encouragingly, the PT, Fbg, APTT and TT of the dogs returned to initial levels by 2 h after the end of the treatment, and the coagulation functions of the dogs remained at normal levels until 24 h after the end of the treatment. Ca^{2+} is an important coagulation factor. As Fig. 5E shows, the concentrations of Ca^{2+} were slightly decreased during the hemoperfusion, which might be due to the chelation between Ca^{2+} and $–COO^-$ of the RAHMs. Moreover, the concentrations of Ca^{2+} were recovered to 80% of the initial levels at 2 h after the end of the treatment, and at 24 h after the end of the treatment, the concentrations of Ca^{2+} were returned to the initial levels. The dogs showed no signs of hypocalcemia during hemoperfusion; therefore, no extra Ca^{2+} was replenished. For patients with regular hemoperfusion treatment (3 or 5 times a week), calcium gluconate could be given intravenously at the end of treatment.

Overall, the results demonstrated that the "anticoagulant + column" with 120 mL solid anticoagulant microspheres could support at least 3 h of whole blood hemoperfusion in hyperbilirubinemia beagles with only an initial dose of heparin.

3.4.3. *Biosafety of the anticoagulant + column*

It is of great importance to perform blood count assays to evaluate the biosafety of biomaterials. As Fig. 6A shows, the RBC levels decreased slightly during the first 15 min and then fluctuated steadily during the 3 h of hemoperfusion therapy. The WBC and PLT levels decreased significantly during the first 45 min and then gradually increased to initial levels by 24 h after the end of the treatment. The transient decline in WBCs and PLTs is common in clinic, which might be due to the activation of the complement system and the excessive use of heparin. Generally, it is not necessary to stop the treatment of hemoperfusion, and appropriate intravenous injection of dexamethasone and oxygen inhalation could relieve the discomfort of patients. The levels of HGB and HCT decreased slightly during the first 15 min and then slowly increased (Fig. 6B), which demonstrated that the microspheres did not cause hemolysis. The slight decline might be caused by the dilution of normal saline in external circulation tubes.

Bilirubin is an albumin-binding toxin. As Fig. 6C shows, the levels of serum total protein (TP), albumin (ALB), and globulin (GLB) were decreased by approximately 20% during hemoperfusion. After hemoperfusion, the levels of TP, ALB and GLB were gradually returned to their initial levels. The decrease in albumin also indicated that the KPMs could also remove some protein-bound toxins. The renal function indexes (Fig. 6D) showed that the concentrations of urea (UREA) and creatinine (CREA) decreased slightly during the first 15 min and then rose gradually to the initial levels. The slight decline might be due to the dilution effect of normal saline. The electrolyte indexes of K^+, Na^+, and Cl^- were not significantly different compared to the pretreatment values (Fig. 6E). Moreover, the concentrations of cholesterol (CHOL) and low-density lipoprotein cholesterol (LDL-C) were slightly decreased, and the concentrations of triglyceride (TG) were not significantly different compared to the pretreatment values (Fig. 6F).

In addition, the dogs survived at least 31 days after hemoperfusion, and the dogs were in good condition (Movie S1). These results further demonstrated the good biosafety of the anticoagulant + column.

Supplementary data related to this article can be found at https://doi.org/10.1016/j.bioactmat.2022.06.019.

4. Conclusion

In conclusion, this is the first trial of a wearable artificial liver to perform in hyperbilirubinemia beagle models without systemic heparinization treatment. Sixty percent heparin could be reduced with 120

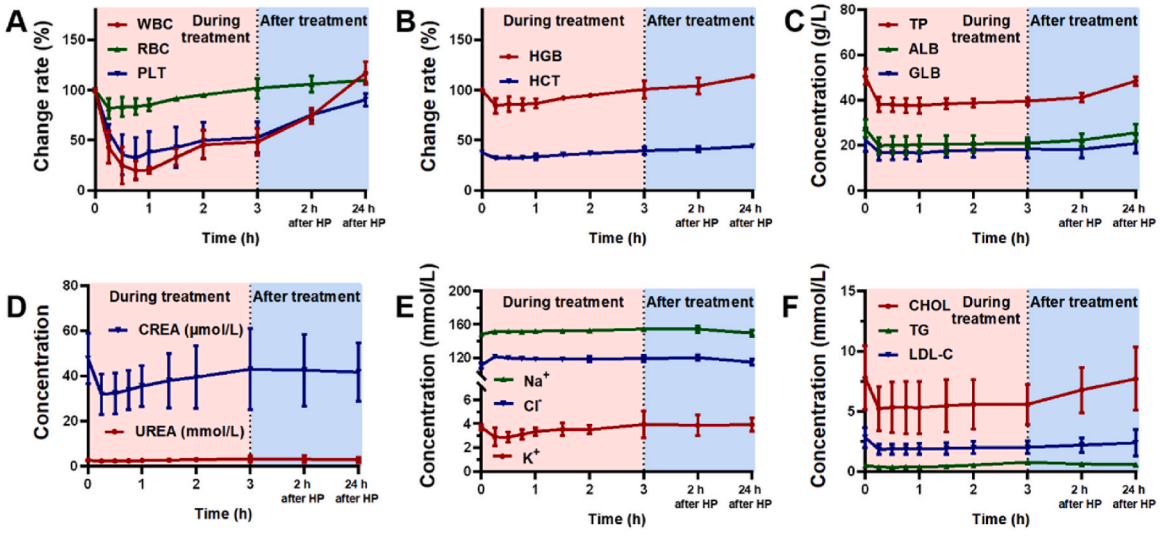

Fig. 6. Biosafety of the "anticoagulant + column" without systemic heparinization treatment in whole blood hemoperfusion. (A and B) Routine blood test during hemoperfusion and after hemoperfusion (n = 3). (C–F) Blood biochemistry analysis during hemoperfusion and after hemoperfusion (n = 3). WBC: White blood cells, RBC: red blood cell, PLT: platelets, HGB: hemoglobin, HCT: hematocrit, TP: total protein, ALB: albumin, GLB: globulin, UREA: urea, CREA: creatinine, K^+: serum potassium, Na^+: serum sodium, Cl^-: serum chlorine, CHOL: cholesterol, TG: triglyceride, LDL-C: low-density lipoprotein cholesterol.

mL solid anticoagulant microspheres, and the double-deck column could support at least 3 h of treatment in hyperbilirubinemia beagles without thrombogenesis. Moreover, the coagulation function of dogs gradually recovered during the treatment. Conceivably, with the increase in solid anticoagulant microspheres or reduce the hemoperfusion time, the column might support hemoperfusion without an initial dose of heparin. Importantly, the removal efficiencies of the double-deck column to total bilirubin (TBIL) were 31.4% in whole blood hemoperfusion, and the concentrations of alkaline phosphatase (ALP), alanine aminotransferase (ALT), aspartate aminotransferase (AST) and γ-glutamyl transpeptidase (GGT) were also decreased approximately 25% after treatment, which suggested that the KPMs could remove several toxins from whole blood and reduce liver damage. Taken together, the design of the "anticoagulant + column" could maximize both the anticoagulant and toxin removal functions *in vivo*. Furthermore, the RAHMs and KPMs were low cost and easy to fabricate on a large scale. We anticipate that the multifunctional column could guide the design of wearable artificial livers for patient care.

5. Outlook

According to the results of this work, we think that the "anticoagulant + column" will be an important direction for the development of wearable artificial livers. Combining different kinds of microspheres into a column instead of fabricating multifunctional microspheres could maximize both the anticoagulant and toxin removal efficiencies and reduce the difficulty of development. Furthermore, different adsorbent microspheres could be assembled with solid anticoagulant microspheres to treat different diseases.

The use of solid anticoagulant microspheres instead of water-soluble anticoagulants could mitigate coagulation-related complications in liver failure patients. Currently, anticoagulant strategies mainly include heparin-like polymers [30], fluoride coatings [31] and anticoagulant-loaded strategies [32]. The development of solid anticoagulant microspheres has achieved several hours of anticoagulation without heparin *in vivo* [14], which can supersede the heparin pump and reduce the weight of the wearable artificial liver device. On the other hand, the anticoagulant coatings in extracorporeal circulation blood tubes could avoid the use of heparin saline prefilling, which will be a vital issue in the realization of free anticoagulant medications dialysis. In evaluating the availability of new anticoagulant materials in the future, more attention should be given to the recovery of coagulation functions after treatment, continuous anticoagulant time and anticoagulant mechanism.

It is difficult for sorbents to compete with albumin to adsorb toxins since most toxins (such as bilirubin, creatinine, indoxyl sulfate, etc.) are albumin-bounded. The adsorption of toxins inevitably leads to a decrease in protein content and may cause blockage of sorbent channels, even activating the immune system. We summarized some bilirubin sorbents regarding their adsorption capacity, fabrication method, cost of materials and *in vivo* clearance efficiency. As Table S6 shows, some sorbents were evaluated for the bilirubin adsorption amount in PBS, and the influence of protein was ignored. Meanwhile, studies based on the establishment of hyperbilirubinemia animal models and the evaluation of biocompatibility *in vivo* are relatively rare. The difficulty in conducting animal experiments may come from difficult fabrication methods for sorbents, expensive raw materials, and less experience in the establishment of animal models. In future sorbent evaluations, successful sorbents should exhibit higher toxin removal efficiency and specificity but also possess excellent biosafety *in vivo*. The increase in adsorption capacity could reduce the amount of microspheres and reduce the volume of the column. The improvement of specificity could reduce the influence of the sorbents on other blood components (such as proteins, ionic equilibrium, immune system). Moreover, blood compatibility problems of the new sorbents should also be considered and addressed since the sorbents are used in whole blood.

Herein, we consulted our clinical consultant, and we found that our research still has the following limitations that have not been solved thus far. (1) The proposed principle machine of wearable artificial liver lacked smart devices, and the smart devices with blue tooth needs to be connected to monitor the patient from the clinic or remotely. (2) The safety of the "anticoagulant + column" has not been verified in animal models with coagulation disorders. (3) At present, we cannot preserve vascular access on laboratory animals. The dogs can only receive a single hemoperfusion treatment, but a single hemoperfusion treatment cannot account for the effect on survival rate. (4) With our existing experimental technologies, only a subacute animal model can be established, which has a very low mortality and is convenient for follow-up treatment and monitoring. If we establish an acute liver failure animal model, strict ventilation technology and anesthesia technology in intensive care facilities are required to avoid nonhuman factor death of experimental animals. These limitations will be solved in our future studies.

The wearable artificial liver is a systems engineering application. Solid anticoagulants and sorbents are the key components to realize safe and efficient toxin removal. Ultimately, safety and user acceptance will be crucial for the transformative adoption of a wearable artificial liver. The treatment mode has changed from "disease-centered" to "patient-centered". For patients in the real world, safe blood access, safe anticoagulant strategy, convenience and price will be essential for patient adoption. Finally, the truly disruptive wearable artificial liver will be an all-round product, as Fig. 7 shows.

Evaluation of the biocompatibility of the KPMs *in vitro*

The experiments were approved and performed by West China Hospital, Sichuan University, and all the experiments were performed in compliance with the relevant laws and national guidelines (GB/T 16886.4-2003/ISO 10993–4:2002, General Administration of Quality Supervision, Inspection and Quarantine of the People's Republic of China, Standardization Administration of the People's Republic of China). Informed consent was obtained for any experimentation with human subjects, and all regulations (e.g., IRB) were fulfilled for using human blood.

Animal experiment

The procedures involving the use of animals in this study were prospectively reviewed and approved by the Institutional Animal Care and Use Committee. This study was conducted in accordance with the National Institutes of Health Guide for the Care and Use of Laboratory Animals (NIH Publications No. 8023, revised 1978). The experiments

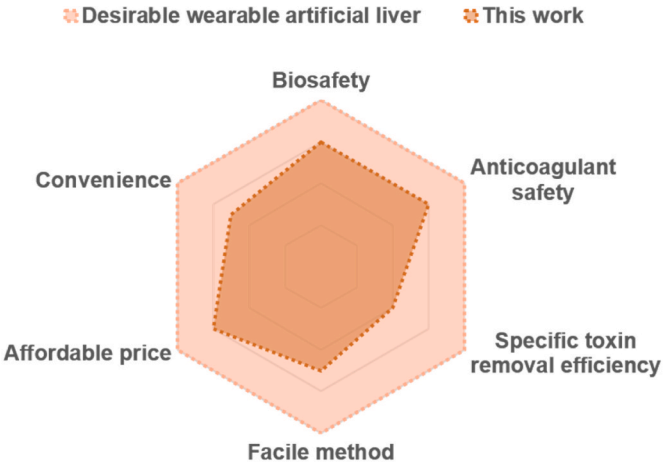

Fig. 7. Characteristics of a desirable wearable artificial liver and the assessment of the "anticoagulant + column" in this work.

conformed to the legal requirements in China and were approved by the ethical committee (No. 2021911A) of West China Hospital, Sichuan University. During the experimental period, the animals had free access to water and food.

CRediT authorship contribution statement

Yilin Wang: proposed the idea and designed the experiments, performed the experiments, characterization and results analysis, wrote and edited the manuscript. **Shanshan Wang:** performed the experiments, characterization and results analysis. **Xueqin He:** assisted with the animal experiment. **Yupei Li:** assisted with the animal experiment. **Tao Xu:** assisted with the fabrication of RAHMs, assisted with the animal experiment. **Lin Xu:** assisted with the animal experiment. **Bo Yang:** assisted with the fabrication of RAHMs, assisted with the animal experiment. **Xinnian Fan:** provided the Kevlar III polymer solution, All authors discussed the results and commented on the manuscript. **Weifeng Zhao:** proposed the idea and designed the experiments, wrote and edited the manuscript, supervised, the whole project. **Changsheng Zhao:** proposed the idea and designed the experiments, wrote and edited the manuscript, supervised, the whole project.

Declaration of competing interest

The authors declare that they have no known competing financial interests or personal relationships that could have appeared to influence the work reported in this paper.

Acknowledgments

The authors would like to thank Chao He at the College of Polymer Science and Engineering, Sichuan University for his generous help with the cryo-electron microscopy test and analysis. Yanping Huang at the College of Chemistry and Engineering, Sichuan University, is thanked for her kind support for the SEM analysis. This work was supported by the National Natural Science Foundation of China (Nos. 52073190, 52122306, 51873115 and U21A2098). The graphics in this work were created with the software tool BioRender.

Appendix A. Supplementary data

Supplementary data to this article can be found online at https://doi.org/10.1016/j.bioactmat.2022.06.019.

References

[1] V. Arroyo, R. Moreau, P.S. Kamath, R. Jalan, P. Ginès, F. Nevens, J. Fernández, U. To, G.G. Tsao, B. Schnabl, A cute-on-chronic liver failure in cirrhosis, Nat. Rev. Dis. Prim. 2 (2016), 16042, https://doi.org/10.1038/nrdp.2016.42.

[2] H.P. Schwartz, B.E. Haberman, R.M. Ruddy, Hyperbilirubinemia current guidelines and emerging therapies, Pediatr. Emerg. Care 27 (9) (2011) 884–889, https://doi.org/10.1097/PEC.0b013e31822c9b4c.

[3] L. Vitek, C. Tiribelli, Bilirubin: the yellow hormone? J. Hepatol. 75 (6) (2021) 1485–1490, https://doi.org/10.1016/j.jhep.2021.06.010.

[4] M.V. Fargo, S.P. Grogan, A. Saguil, Evaluation of jaundice in adults, Am. Fam. Physician 95 (3) (2017) 164–168.

[5] V. Fuhrmann, M. Bauer, A. Wilmer, The persistent potential of extracorporeal therapies in liver failure, Intensive Care Med. 46 (3) (2020) 528–530, https://doi.org/10.1007/s00134-019-05886-6.

[6] J.C. Lai, N.N. Ufere, J.C. Bucuvalas, Liver transplant survivorship, Liver Transplant. 26 (8) (2020) 1030–1033, https://doi.org/10.1002/lt.25792.

[7] P. Konstantin, J. Chang, V. Otto, G. Brunner, Artificial liver, Artif. Organs 16 (3) (1992) 235–242, https://doi.org/10.1111/j.1525-1594.1992.tb00303.x.

[8] M.P. van de Kerkhove, R. Hoekstra, T.M. van Gulik, R.A.F.M. Chamuleau, Large animal models of fulminant hepatic failure in artificial and bioartificial liver support research, Biomaterials 25 (9) (2004) 1613–1625, https://doi.org/10.1016/S0142-9612(03)00509-X.

[9] F.P. Hessel, Economic evaluation of the artificial liver support system MARS in patients with acute-on-chronic liver failure, Cost effectiveness and resource allocation, C/E 4 (2006) 16, https://doi.org/10.1186/1478-7547-4-16.

[10] K. Shirane, H. Funakubo, K. Tohyama, A. Takeuchi, Fundamental Studies on Wearable Artificial Kidney and Liver. Long-Term Blood Filtration Efficiency of Nuclepore Membrane Filter with Pore-Size of 0.6 Mu, vol. 37, Annual Report of the Engineering Research Institute, Faculty of Engineering, University of Tokyo, 1978, pp. 69–74.

[11] F.F. Violi, Domenico, Stefania Basili, Coagulopathy of chronic liver disease, N. Engl. J. Med. 365 (15) (2011) 1452–1454, https://doi.org/10.1056/NEJMc1109231.

[12] J.J. García Martínez, K. Bendjelid, Artificial liver support systems: what is new over the last decade? Ann. Intensive Care 8 (1) (2018) 109, https://doi.org/10.1186/s13613-018-0453-z.

[13] X. Song, T. Xu, L. Yang, Y. Li, Y. Yang, L. Jin, J. Zhang, R. Zhong, S. Sun, W. Zhao, C. Zhao, Self-anticoagulant nanocomposite spheres for the removal of bilirubin from whole blood: a step toward a wearable artificial liver, Biomacromolecules 21 (5) (2020) 1762–1775, https://doi.org/10.1021/acs.biomac.9b01686.

[14] X. Song, H. Ji, Y. Li, Y. Xiong, L. Qiu, R. Zhong, M. Tian, J.N. Kizhakkedathu, B. Su, Q. Wei, W. Zhao, C. Zhao, Transient blood thinning during extracorporeal blood purification via the inactivation of coagulation factors by hydrogel microspheres, Nat. Biomed. Eng. 5 (2021) 1143–1156, https://doi.org/10.1038/s41551-020-00673-x.

[15] J. Zhu, M. Yang, A. Emre, J.H. Bahng, L. Xu, J. Yeom, B. Yeom, Y. Kim, K. Johnson, P. Green, N.A. Kotov, Branched aramid nanofibers, Angew. Chem. Int. Ed. 56 (39) (2017) 11744–11748, https://doi.org/10.1002/anie.201703766.

[16] Y. Yang, S. Yin, C. He, X. Wu, J. Yin, J. Zhang, L. Ma, W. Zhao, C. Cheng, C. Zhao, Construction of Kevlar nanofiber/graphene oxide composite beads as safe, self-anticoagulant, and highly efficient hemoperfusion adsorbents, J. Mater. Chem. B 8 (9) (2020) 1960–1970, https://doi.org/10.1039/c9tb02789k.

[17] Z. Peng, Y. Yang, J. Luo, C. Nie, L. Ma, C. Cheng, C. Zhao, Nanofibrous polymeric beads from aramid fibers for efficient bilirubin removal, Biomater. Sci. 4 (9) (2016) 1392–1401, https://doi.org/10.1039/c6bm00328a.

[18] Y. Wang, X. Huang, C. He, Y. Li, W. Zhao, C. Zhao, Design of carboxymethyl chitosan-based heparin-mimicking cross-linked beads for safe and efficient blood purification, Int. J. Biol. Macromol. 117 (2018) 392–400, https://doi.org/10.1016/j.ijbiomac.2018.05.091.

[19] C. Nie, Z. Peng, Y. Yang, C. Cheng, L. Ma, C. Zhao, Kevlar based nanofibrous particles as robust, effective and recyclable absorbents for water purification, J. Hazard Mater. 318 (2016) 255–265, https://doi.org/10.1016/j.jhazmat.2016.06.061.

[20] C. Xie, Z.X. Guo, T. Qiu, X. Tuo, Construction of aramid engineering materials via polymerization-Induced para-aramid nanofiber hydrogel, Adv. Mater. 33 (31) (2021), 2101280, https://doi.org/10.1002/adma.202101280.

[21] C. Yang, H. Wu, Y. Dai, D. Zhang, R. Xu, L. Luo, X. Liu, Constructing mainstay-body structure in heterocyclic aramid fiber to simultaneously improve tensile strength and toughness, Compos. Part. B-eng. 202 (2020), 108411, https://doi.org/10.1016/j.compositesb.2020.108411.

[22] R. Zhao, T. Ma, F. Cui, Y. Tian, G. Zhu, Porous aromatic framework with tailored binding sites and pore sizes as a high-performance hemoperfusion adsorbent for bilirubin removal, Adv. Sci. 7 (23) (2020), https://doi.org/10.1002/advs.202001899, 2001899.

[23] M. Matsushita, T. Fujita, Activation of the classical complement pathway by mannose-binding protein in association with a novel C1s-like serine protease, J. Exp. Med. 176 (6) (1992) 1497–1502, https://doi.org/10.1084/jem.176.6.1497.

[24] U. Delbalzo, M.J. Polley, R. Levi, C3a-induced contraction of Guinea-pig ileum consists of 2 components-fast histamine-mediated and slow prostanoid-mediated, J. Pharmacol. Exp. Therapeut. 248 (3) (1989) 1003–1009.

[25] D. Ricklin, G. Hajishengallis, K. Yang, J.D. Lambris, Complement: a key system for immune surveillance and homeostasis, Nat. Immunol. 11 (9) (2010) 785–797, https://doi.org/10.1038/ni.1923.

[26] J. Sorgenfrei, B. Damerau, W. Vogt, Role of histamin in the spasmogenic effect of the complement peptides C3a and C5a-desarg (classical anaphylatoxin), Agents Actions 12 (1982) 118–121, https://doi.org/10.1007/bf01965121.

[27] A.R. Hamoud, L. Weaver, D.E. Stec, T.D. Hinds Jr., Bilirubin in the liver-gut signaling axis, Trends Endocrinol. Metabol. 29 (3) (2018) 140–150, https://doi.org/10.1016/j.tem.2018.01.002.

[28] J.D. Ostrow, P. Mukerjee, C. Tiribelli, Structure and binding of unconjugated bilirubin-relevance for physiological and pathophysiological function, J. Lipid Res. 35 (10) (1994) 1715–1737, https://doi.org/10.1016/S0022-2275(20)39768-6.

[29] Y. Chai, Z. Liu, Y. Du, L. Wang, J. Lu, Q. Zhang, W. Han, T. Wang, Y. Yu, L. Sun, L. Ou, Hydroxyapatite reinforced inorganic-organic hybrid nanocomposite as high-performance adsorbents for bilirubin removal in vitro and in pig models, Bioact. Mater. 6 (12) (2021) 4772–4785, https://doi.org/10.1016/j.bioactmat.2021.05.017.

[30] C. He, H. Ji, Y. Qian, Q. Wang, X. Liu, W. Zhao, C. Zhao, Heparin-based and heparin-inspired hydrogels: size-effect, gelation and biomedical applications, J. Mater. Chem. B 7 (8) (2019) 1186–1208, https://doi.org/10.1039/c8tb02671h.

[31] D.C. Leslie, A. Waterhouse, J.B. Berthet, T.M. Valentin, A.L. Watters, A. Jain, P. Kim, B.D. Hatton, A. Nedder, K. Donovan, E.H. Super, C. Howell, C.P. Johnson, T.L. Vu, D.E. Bolgen, S. Rifai, A.R. Hansen, M. Aizenberg, M. Super, J. Aizenberg, D.E. Ingber, A bioinspired omniphobic surface coating on medical devices prevents thrombosis and biofouling, Nat. Biotechnol. 32 (11) (2014) 1134–1140, https://doi.org/10.1038/nbt.3020.

[32] C.J. Pan, L.Q. Pang, F. Gao, Y.N. Wang, T. Liu, W. Ye, Y.H. Hou, Anticoagulation and endothelial cell behaviors of heparin-loaded graphene oxide coating on titanium surface, Mater. Sci. Eng. C 63 (2016) 333–340, https://doi.org/10.1016/j.msec.2016.03.001.